ADVANCED FUNCTIONAL MATERIALS

FULL PAPER

DOI: 10.1002/adfm.200800637

# Hierarchical Superstructures with Helical Sense in Self-Assembled Achiral Banana-Shaped Liquid Crystalline Molecules**

By *Shih-Chieh Lin, Tz-Feng Lin, Rong-Ming Ho,* Chin-Yen Chang,* and *Chain-Shu Hsu**

The self-assembly of 1,3-phenylene bis[4-(4-*n*-heptyloxybenzoyloxy)-benzoates] (BC7) is studied to examine the formation of helical morphologies from achiral banana-shaped liquid crystal molecules at different self-assembling levels. Various hierarchical superstructures including flat-elongated lamellar crystal, left- and right-handed helical ribbons, and tubular texture are observed while the BC7 molecules self-assemble in THF/$H_2O$ solution. By contrast, only plate-like morphology is observed in the self-assembly of achiral linear shaped 1,4-phenylene bis[4-(4-*n*-heptyloxybenzoyloxy)-benzoates] (LC7) molecules, indicating that the chirality of the self-assembled texture is strongly dependent upon the molecular geometry of the achiral molecules. The formation of the helical superstructures, namely hierarchical chirality, is attributed to the conformational chirality from the achiral banana-shaped liquid crystalline molecules, as evidenced by significant optical activity in time-resolved circular dichroism experiments. Selective area electron diffraction is performed to examine the structural packing of the hierarchical superstructures. As observed, the molecular disposition of the lamellar crystal is identical to that of the helical superstructure. Also, the diffraction patterns of the helical superstructures appeared arc-like patterns consisting of a series of reflections, suggesting that the helical morphology resulted from the curving of the lamellar crystals through a twisting and bending mechanism. Consequently, the model of molecular disposition in the self-assembled helical superstructures from the achiral banana-shaped molecules is proposed. The morphological evolution in this study may provide further understanding with respect to the chiral information transfer mechanism from specific molecular geometry to hierarchical chirality in the achiral banana-shaped molecules.

## 1. Introduction

Nature uses self-assembly to construct materials with specific functions from molecular level by non-covalent interactions (i.e., the secondary forces) including hydrogen bonding, amphiphilic effect, polar ability, electrostatic interaction, ionic bonding, metal coordination, van der Waals force, $\pi$–$\pi$ stacking, steric effect and chirality.[1–4] Among the biological architectures formed by self-assembly, helical morphology is probably the most fascinating texture in nature. A variety of helical morphologies in the self-assembled architectures including helical chain conformation, hierarchical helical superstructure and helical crystalline phase have been observed and studied.[5–17] It is known that the helical superstructures are formed in the hierarchical organization of chiral molecules. However, the mechanisms of transferring chiral information from one structural level to another are still in debate, and have been proven to be much more complicate than one usually predicts.

In contrast to helical morphologies formed in the chiral liquid crystalline molecules,[18–24] the specific phase chirality (i.e., banana phase) may also be obtained from achiral banana-shaped molecules (i.e., bent-core structures without chiral entity).[25–27] Vorländer and co-workers examined the mesogenic behavior in the first time at which ortho-, meta-, and para-substituted dihydroxybenzene diesters possessing two azoxybenzene mesogenic units were synthesized and the effect of molecular geometry on mesogenicity were studied.[28] Pelzl and coworkers reinvestigated these dihydroxybenzene diesters, and demonstrated the existence of the banana phase within the meta-substituted isomer, termed $B_6$.[29–31] This meta-substituted isomer is now regarded as the first banana-phase mesogen. Since Niori and co-workers reported ferroelectric switching behavior in the smectic phase of achiral banana-shaped Schiff-based derivatives[32,33] (the mesophase has been demonstrated as antiferroelectricity later),[34,35] the unconventional mesomorphic properties of the unique banana liquid crystal phases have attracted great attention over the past few years. The macroscopic chirality of the achiral banana-

[*] Prof. R.-M. Ho, S.-C. Lin, T.-F. Lin
Department of Chemical Engineering, National Tsing Hua University
Hsinchu 30013 (Taiwan)
E-mail: rmho@mx.nthu.edu.tw
Prof. C.-S. Hsu, C.-Y. Chang
Department of Applied Chemistry, National Chiao Tung University
Hsinchu 30010 (Taiwan)
E-mail: cshsu@mail.nctu.edu.tw

Authors would like to thank Prof. Y.-S. Yang of Department of Biological Science and Technology, National Chiao Tung University for his help in circular dichroism (CD) experiments. We also appreciate Ms. P.-C. Chao of Regional Instruments Center at National Chung Hsing University for her help in transmission electron microscopy (TEM) experiments. This work is supported by the National Science Council (NSC97-2221-E-007-035-MY3). Supporting Information is available online from Wiley InterScience or from the authors.

ADVANCED FUNCTIONAL MATERIALS



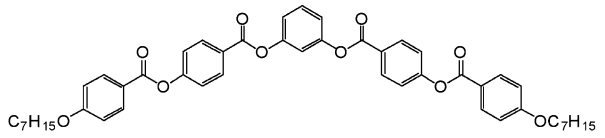


1,3-phenylene bis[4-(4-n-heptyloxybenzoyloxy) benzoates] (BC7)

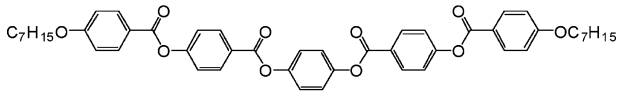


1,4-phenylene bis[4-(4-n-heptyloxybenzoyloxy)-benzoates] (LC7)

**Scheme 1.** Chemical Structures of BC7 and LC7.

shaped molecules can be observed in their unique mesophases such as $B_2$ phase with electro-optical switchable property (the smectic layered chirality induced by the existence of the polar direction and the tilting molecular director with respect to the layer normal)[36–40], $B_4$ phase with opposite optical activity (the different chiral domains formed from the helical morphology which is similar to the twist grain boundary phase),[41–44] and $B_7$ phase with macroscopic spiral and more complicated textures.[45–49] Watanabe and co-workers suggested that the asymmetric twisting conformation which is resulted from the ester linkage groups connecting the central phenyl ring with the side wings seems to be one of the origins for the formation of the helical morphology.[50–55] By contrast, different mechanisms, such as the twisting power induced by an offset to the macroscopic polarization and the construction of an enantiomorphoic structure by tilting of molecules with respect to the layer normal, have also been proposed.[56–59] Although various types of achiral banana-shaped liquid crystalline molecules have been synthesized and studied in their unique liquid crystal phases, the mechanisms for the formation of helical superstructures from the molecular level to the hierarchical level is still challenging.

In this study, a typical kind of achiral banana-shaped liquid crystalline molecule, 1,3-phenylene bis[4-(4-*n*-heptyloxybenzoyloxy) benzoates] (BC7, i.e., bent-core structure with terminal alkyl chain length $n = 7$), was synthesized to examine the mechanisms of the induced chirality by the bent-core structures at different self-assembling levels whereas an achiral linear shaped molecule, 1,4-phenylene bis[4-(4-*n*-heptyloxybenzoyloxy)-benzoates] (LC7), was also synthesized for comparison (Scheme 1). We aim to inspect the self-assembly from the molecular level to hierarchical level, so as to build up the evolution of helical morphology at different self-assembling levels.

## 2. Results and Discussion

### 2.1. Self-Assembly of Achiral Banana-Shaped Molecules in Solution

Considering the specific shape effect which results in the symmetry-breaking with twisting conformation on the self-assembly of achiral banana-shaped liquid crystalline molecules, circular dichroism (CD) and UV-Vis spectroscopic measurements were performed to investigate the optical activity of self-assembled textures and corresponding aggregation mechanisms in solution. To determine the optical activity information of single-chain conformation, dilute solution was prepared. The concentration of the dilute solution was both $1.6 \times 10^{-5}$ M in UV-Vis and CD experiments. Figure 1 shows the UV-Vis and CD results of BC7 dissolved in THF solution. The maximum absorption of $\pi$–$\pi^*$ transition for the phenyl chromophores in UV-Vis appears at 264 nm (Fig. 1a). In CD results, it is expected that there is no obvious optically active signal appearing for single-chain conformation in dilute solution as BC7 is achiral (Fig. 1b). In contrast to the nil optical activity of BC7 single-chain conformation, optical activity gradually appears and eventually well develops after the introduction of $H_2O$ in the solution (i.e., THF/$H_2O$ = 1.2 v/v) as shown in the time-resolved CD measurement (Fig. 2a). It is intuitive to suggest that the appearance of optical activity is attributed to the aggregation of the achiral BC7 molecules because of the $H_2O$ immiscibility with respect to the BC7 molecules. As shown, the sharp peak at 296 nm appears and constantly remains once the aggregation time reaches a certain

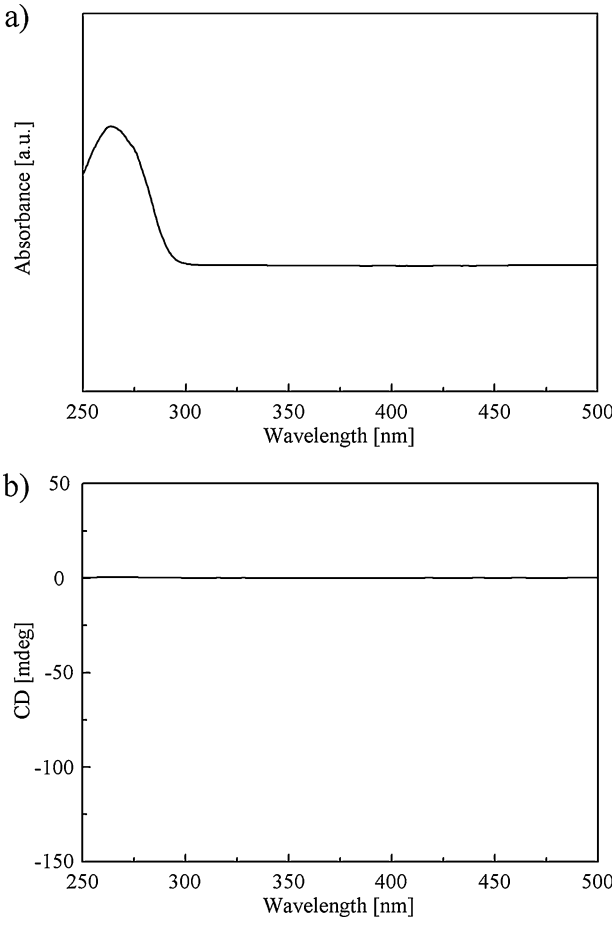


**Figure 1.** a) UV-Vis; b) CD spectra of BC7 in THF dilute solution. The concentration in UV-Vis and CD measurements is $1.6 \times 10^{-5}$ M.

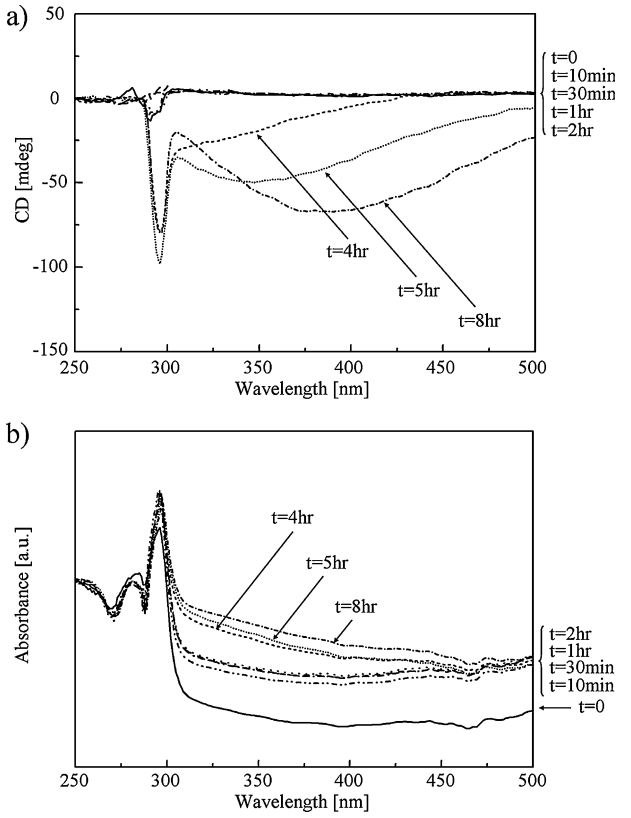


**Figure 2.** a) Time-resolved CD; b) corresponding absorption spectra of BC7 self-assembly in THF/$H_2O$ solution. Significant CD signals appear after four-hour aggregation. (THF/$H_2O$ = 1.2 v/v and [BC7] = 0.048 wt%)

level whereas a broad peak beyond 300 nm gradually appears and then shifts to longer wavelength region with time in the process of aggregation (i.e., the self-assembly process). We suggest that the characteristic peak at 296 nm is attributed to the absorption from the BC7 molecules organized into helical hierarchical superstructure because this very sharp absorption with significant red shifting as compared to single-chain molecular absorption after aggregation is the characteristic of J-aggregation.[60,61] Hence, the red shifting of the absorption band in CD spectra indicates the existence of the chiral J-aggregates, and can be accounted for the signature of intermolecular $\pi$-$\pi$ interaction from the helical chain conformation.[62,63] It is noted that those CD signals in Figure 2a may involve the absorption from the organized molecules and also the Bragg reflection from the periodic pitch length of the helical superstructure which occurs in cholesteric liquid crystal phase. Comparing the CD and absorption spectra, the sharp peak at 296 nm in CD is thus referred to the absorption of BC7 molecules since this signal also appears in absorption measurement (Fig. 2b). By contrast, the broad peak beyond 300 nm in CD spectra is assigned as the Bragg reflection because there is no obvious and specific signal in absorbance spectra at the nearby absorptions and the pitch length of the hierarchical morphologies is approximately equivalent to the wavelength of the incident circular polarized light. It is also noted that only exclusive Cotton effect (i.e., either negative or positive responses) can be identified for the aggregates. Based on the chiral symmetry breaking, the BC7 molecules may spontaneously break symmetry and select a handedness.[64,65] We speculate that there is equal population for symmetry breaking transition of BC7 molecules with self-assembly at initial stage. However, once the left- or right-handed conformation becomes dominative with respect to the other (i.e., more population in concentration), the specific optical activity from the induced chiral conformation will be expressed and followed by the selection of handedness for the final morphology, similar to the prediction of the majority rule.[66–68] We thus speculate that the change of CD results with self-assembly process is in accordance with the evolution of hierarchical formation.

### 2.2. Self-Assembled Superstructures in Solution

To further confirm the speculation of the induced chirality by aggregation, the solution of the achiral banana-shaped BC7 molecules in the mixed solvent at different stages for self-assembly (i.e., different aggregation times) were cast onto glass slide and then examined by depolarized light microscopy (DPLM). Interesting morphological evolution can be identified by DPLM (Fig. S3); only micelle-like texture is observed in the beginning but the aggregates of fibrillar texture can be found once the aggregation time is over a specific period. Figure S3d shows the DPLM micrograph of the fibrillar texture with several tens of micrometer-long and hundreds of nanometer-wide dimension organized with the BC7 molecules while significant aggregation occurs. As expected, this time period for the formation of hierarchical morphologies with specific textures corresponds well with the time required for the occurrence of specific response peak in the CD measurement. This correspondence suggests that the formed hierarchical morphologies are responsible for the appearance of optical activity in the BC7 solution.

As evidenced by the spectroscopic analyses, we thus suggest that the achiral banana-shaped molecules gradually aggregate to form morphologies with helical sense in the THF/$H_2O$ solution. The self-assembly is driven by the $\pi$–$\pi$ interaction between the intermolecular mesogeic units to stabilize the morphology. To further examine the hierarchical superstructures from solution, the solution with self-assembled morphologies can be solution cast on the glass slides or carbon-coated glass slides, and then observed by transmission electron microscopy (TEM), scanning electron microscopy (SEM), and scanning probe microscopy (SPM). Figure 3 shows the TEM micrographs of self-assembled aggregates where different hierarchical textures can be found. In addition to flat-elongated lamellar crystals (Fig. 3a), characteristic helical superstructures with different pitch lengths and helicities can be observed (Fig. 3b and c). Also, a tubular superstructure (Fig. 3d) can be obtained. We speculate that the formation of the tubular morphology is attributed to the scrolling mechanism similar to

ADVANCED FUNCTIONAL MATERIALS



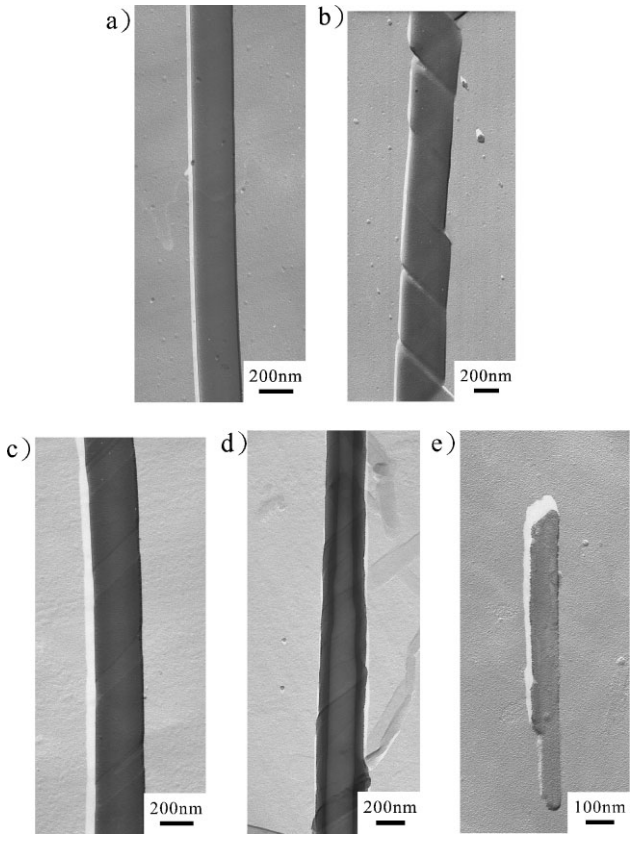


**Figure 3.** TEM images of self-assembled nanostructures from the BC7 molecules in THF/$H_2O$ (1.2 mL/1 mL) solution. a) the flat-elongated lamellar crystal; b) left-handed helical ribbon superstructure; c) right-handed helical ribbon superstructure, and d) tubular superstructure from the helical ribbon structure. e) TEM image of self-assembled nanostructure from the LC7 molecules in THF/$H_2O$ (1.2 mL/1 mL) solution. Only lamellar crystalline structure can be observed.

the results predicted by tilted chiral lipid bilayer (TCLB) theory.[69–73] Consistently, helical trace line can be clearly recognized on the exterior of the tubular superstructure; further confirming the proposed scrolled mechanism.

Because of the achiral property of the intrinsic chemical structure of the banana-shaped liquid crystalline molecules, the induced chirality by the shape effect of the achiral banana-shaped liquid crystalline molecules may exhibit equal population of left- and right-handed helical superstructures as evidenced by Figure 3b and c, respectively. Nevertheless, the formation of the aggregates in solution is a kinetically controlled process so that a variety of hierarchical superstructures with various pitch lengths and both handednesses can be identified. The pitch length variation ranges from 400 nm to 800 nm; consistent to the suggested Bragg reflections from the hierarchical superstructures in previous CD results.

For comparison, the achiral linear shaped molecules, LC7 were synthesized. The maximum absorption of $\pi$–$\pi^*$ transition appears at 267 nm in UV-Vis measurement (Fig. S4a), and the absence of CD signal indicates that the LC7 molecules in THF dilute solution are indeed lack of intrinsic optical activity (Fig. S4b). Furthermore, after the aggregation of the LC7 in the THF/$H_2O$ solution, no specific optical active signal in CD measurements (Fig. S5a) but slight red shift from 267 nm to 274 nm (Fig. S5b) in the corresponding absorption spectra can be found. As a result, different to the self-assembled superstructures from BC7, only lamellar crystalline structure is observed (Fig. 3e); suggesting that LC7 molecules only have parallel face-to-face $\pi$–$\pi$ stacking in molecular packing and the formation of hierarchical chirality in BC7 is truly attributed to the specific molecular regularity (i.e., the induction of conformational chirality due to the bent-core structure).

Interestingly, zigzag morphology and other helical superstructures can also be observed as evidenced by TEM, SEM and SPM (Fig. 4). We speculate that the zigzag morphology is attributed to the collapse of the helical superstructure because of the overwhelming weight from gravity. The thickness of the helical superstructure derived from SPM is analogous with the results calculated from TEM by Pt shadowing. Also, the morphological evolution of self-assembly of the BC7 molecules from platelet-like to helical superstructures can occasionally be observed (Fig. 5); demonstrating the transitional mechanism. It is reasonable to suggest that the observed helical ribbon is resulted from the curving of the flat-elongated lamellar crystal so as to reach a morphological state with higher stability, and eventually form a tubular morphology as observed. The observed hierarchical morphologies with helical sense in the self-assembly of the BC7 indicate that the conformational chirality is related to the specific molecular regularity, and chiral information may transfer from the conformational chirality to the hierarchical chirality through self-assembly.

### 2.3. Structural Determination of Self-Assembled Morphologies

To study the molecular disposition for the formed hierarchical chirality, selected area electron diffraction (SAED) experiments were carried out to examine the structural packing of the self-assembled morphologies. Figure 6a shows a TEM micrograph of the flat-elongated lamellar crystal with the BC7 molecules self-assembling in the THF/$H_2O$ solution whereas [00*l*] zonal selective area electron diffraction pattern can be obtained from the lamellar crystal (Fig. 6b). The basal unit cell dimensions are thus determined as $a = 0.98$ nm and $b = 0.80$ nm. In contrast to the diffraction result of the lamellar crystal, the SAED pattern of the helical hierarchical superstructure exhibits symmetric arcs which consists of a series of reflections (Fig. 6d) and the unit cell possesses the same dimensions with that of the lamellar crystal as further evidenced by X-ray results (detailed structural determination of achiral banana-shaped molecules at crystalline state is still in progress); indicating that the chain packing in crystalline state of the aggregates is identical regardless of the final hierarchical morphology. Also, we speculate that the arc-like diffraction

  

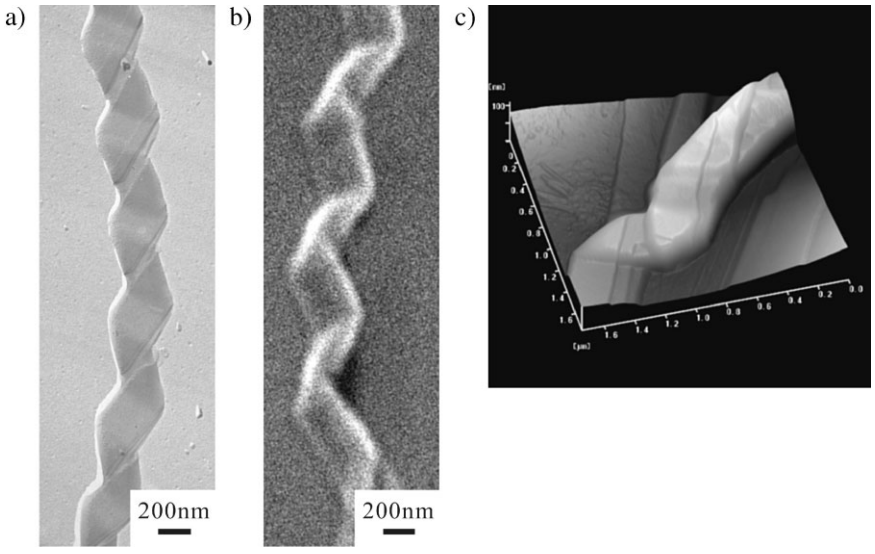


**Figure 4.** a) TEM image; b) SEM image and c) SPM image of the zigzag morphology with BC7 self-assembly in THF/$H_2O$ (1.2 mL/1 mL) solution.

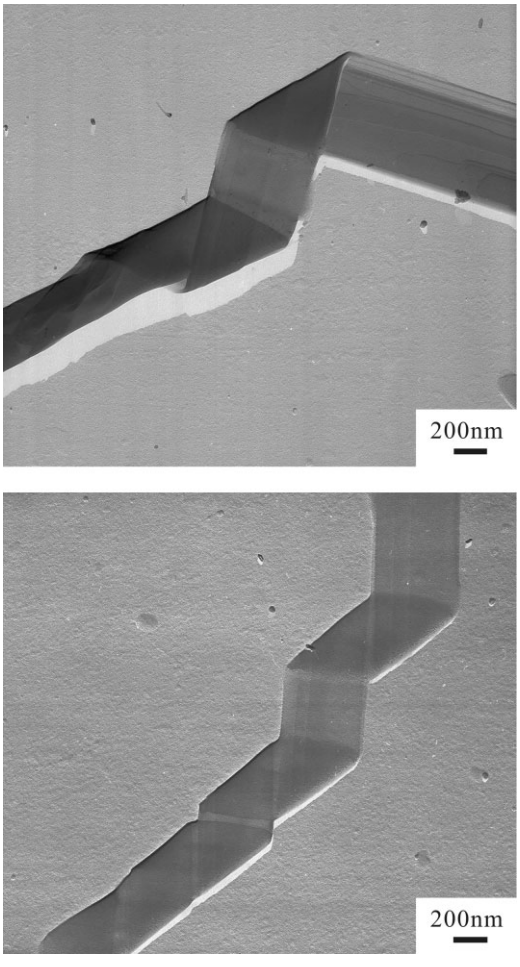


**Figure 5.** TEM image of morphological transition from lamellar crystal to helical superstructure with BC7 self-assembly in THF/$H_2O$ (1.2 mL/1 mL) solution.

pattern consisting of a series of single-crystalline-like reflections (i.e., diffraction spots) is an evidence to infer the twisting and bending mechanism for the formation of the helical superstructures.

Considering the energetic compensation of molecular packing, the helical conformation of achiral banana-shaped molecules is induced in the self-assembly mechanism and provides conformational chirality so as to lead the bending and twisting forces. These helical conformations with the same twist sense are closed packing and form the crystalline nuclei with chiral sense. To minimize energetic penalty from the growth of the flat-elongated lamellar crystal due to the cause of steric effect, these crystallites of helical chains may have a tendency to curve successively and finally form the helical superstructure. However, once the collapse happens due to overweighting of the helical superstructure, the crystalline lattices on the curvature of the helical architecture should fall on the same horizontal level. This collapse process usually makes the upper and lower layers of the helical superstructure perpendicular to each other, which is similar to the formation of the zigzag morphology, and also exhibits the symmetric diffraction patterns with respect to the perpendicular coordinates. As a result, a series of specific reflections resulting from the same crystalline planes of different lattices on the curvature appears together on the same reciprocal plane due to the same horizontal level; it may lead the construction of the arc-like pattern consisting of a series of single-crystal-like reflections with respect to the twisting and bending mechanism. In contrast to the symmetric arc diffraction patterns obtained from the upper and lower layers of helical morphologies, the overlapping lamellar crystals shows only specific reflections (Fig. S6). This difference between the arc-like patterns of the helical superstructure and the specific reflections of the lamellar crystal demonstrates that the absence of twisting and bending mechanism in lamellar crystals.

### 2.4. Proposed Mechanism for the Formation of Self-Assembled Superstructures

Figure 7 illustrates the hypothetic model for the formation of the helical superstructures of the BC7 molecules while self-assembling in the THF/$H_2O$ solution. We speculate that the helical superstructure is initiated by the formation of the conformational chirality of achiral banana-shaped liquid crystalline molecules during aggregation. As reported by Watanabe and coworkers, the molecular chirality is attributed to helical conformation, namely conformational chirality.[50–55]

ADVANCED FUNCTIONAL MATERIALS



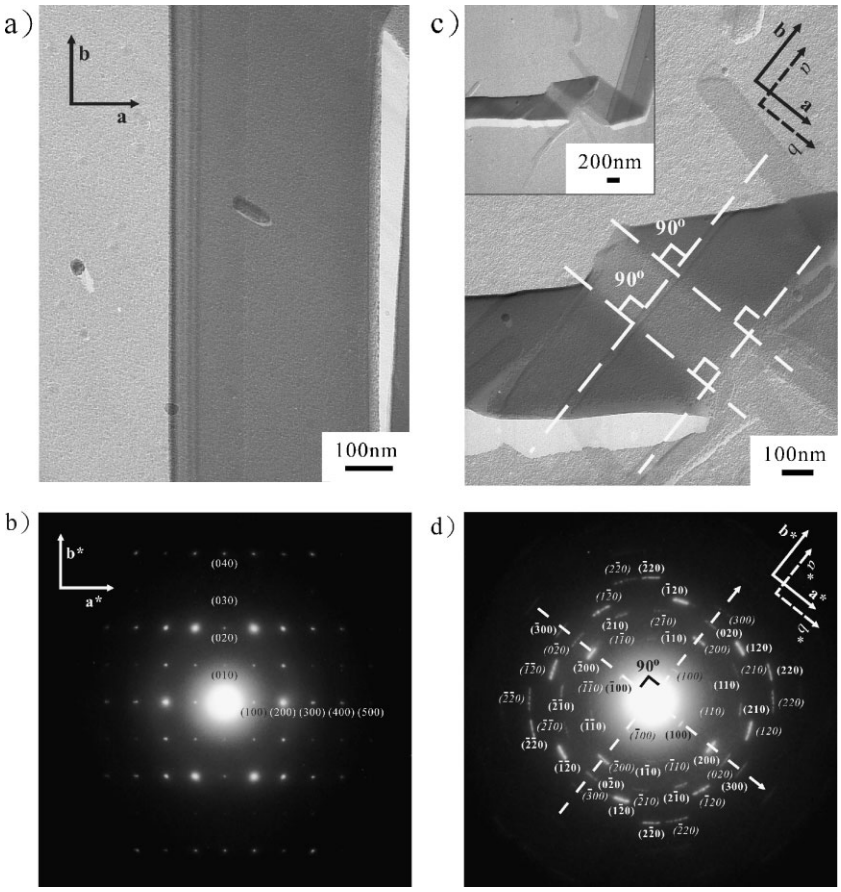


**Figure 6.** TEM images of a) lamellar crystal and c) helical superstructure from the BC7 molecules in THF/$H_2O$ (1.2 mL/1 mL) solution. The insert of c) is a TEM micrograph with low magnification. b) and d) are the selected area electron diffraction (SAED) patterns with respect to a) and c). In d), each arc is constructed with a series of specific single-crystal-like reflections. Straight line with boldface indicates the coordinate of the upper layer and dashed line with italic type refers to that of the lower layer of the helical superstructure in c) and d).

Consistent to our molecular simulation results as shown in Figure 7a, during self-assembly, the most stable conformation of the BC7 molecule can be achieved through chiral aggregation by taking the rotation of carboxyl groups with specific angles, then inducing helical chain conformation with specific helical sense for appropriate molecular packing, as evidenced by the time-resolved CD results.

The morphological evolution of the helical superstructure can also be clearly identified by DPLM observation at which the micelle-like texture is found at the beginning of aggregation, and then helical textures can be observed for long-time aggregation (Fig. S3). As the expectation of the TCLB theory, the spherical vesicles organized by chiral lipid molecules may transform to vesicle fusion, and finally form the aggregated helical superstructure (i.e., twisting stripe or ribbon helices). The described morphological evolution of the helical superstructures above is indeed similar to the observation of self-assembled aggregates of the BC7 molecules in the mixed solvent. At early stage of aggregation, the solvophobic interaction between the banana-shaped liquid crystalline molecules and water is the primary driving force toward aggregation. Subsequently, the forcible packing with $\pi$–$\pi$ stacking will lead the nucleation of flat-elongated lamellar crystals in the beginning. Namely, the helical conformations with the same helical sense are close packing to form the crystallites that gives rise to specific chiral information. Also, according to Spector and co-workers, the chiral molecular packing should impose a steric hindrance to lead the formation of stable structure through twisting and bending mechanism in terms of energetic consideration.[64,65] Consistently, we conjecture that chiral steric effect also occurs in the molecular packing of achiral banana-shaped molecules with chiral symmetry breaking at which the twisting and bending forces between each neighboring molecules lead to the curving of flat-elongated lamellar crystals.

We speculate that the self-assembly of the banana-shaped molecules via $\pi$–$\pi$ interaction can still maintain the molecules to pack closely even with the steric effect because of the slightly twisting and bending in crystallites. With the continuous growth of lamellar crystals, the accumulation of surface free energy attributed to twisting and bending should eventually lead to significant curving of the lamellar crystals (as evidenced by the observation of morphological transition in Fig. 5), namely the formation of the helical superstructures (see Fig. 7b for illustration). Therefore, the bending and twisting of achiral banana-shaped liquid crystalline molecules with helical conformation should occur simultaneously with energetic consideration so as to lower steric hindrance in self-assembly process and lead to the continuous curving of crystalline lamellae. The observed arc-like diffraction pattern consisting of a series of single-crystalline-like reflections (Fig. 6) further identify the growing mechanism of the self-assembled superstructures. The top-view of Figure 7b illustrates the collapsed zigzag morphology that may give a series of specific reflections, (namely, the arc-like diffraction result) because the crystalline lattices on the curvature of the helical architecture exhibit twisting and bending along *b*-axis. Furthermore, to lower the energetic penalty from the edge of helical ribbon, as illustrated in Figure 7c, the helical superstructures may scroll successively for the formation of the tubular superstructure, which is the most stable morphology from the expectation of TCLB theory.

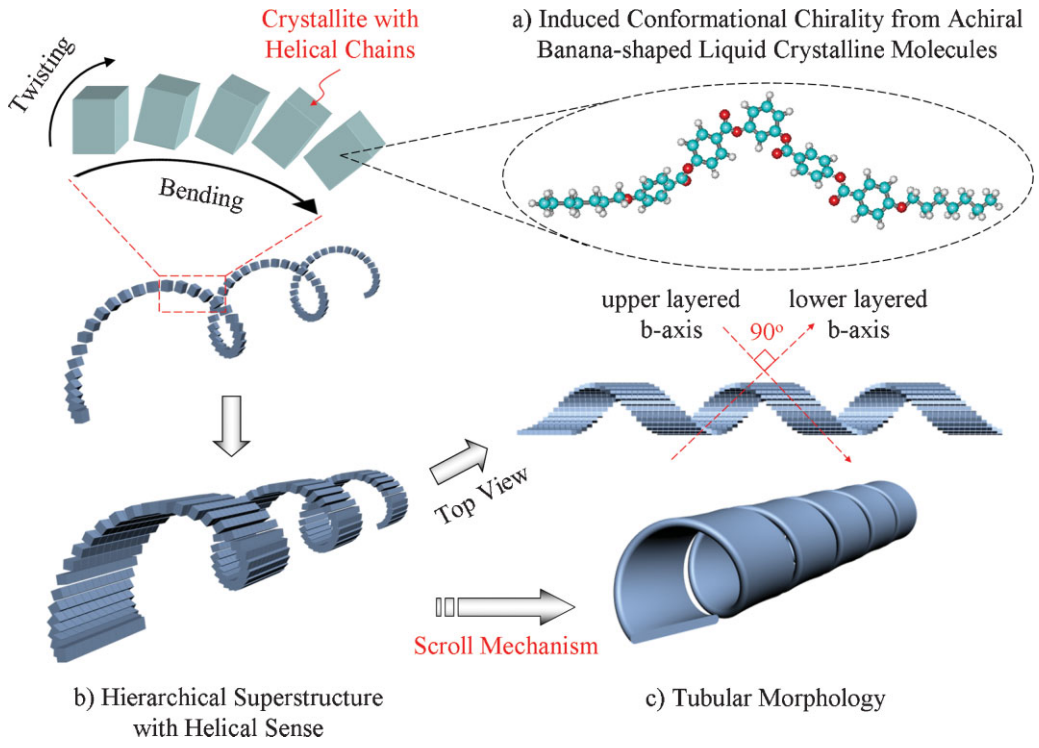


**Figure 7.** Hypothetical model for the formation of a hierarchical helical superstructure with the BC7 molecules. a) The self-assembled aggregation signifies the twisting conformation of achiral banana-shaped liquid crystalline molecules, namely the induced conformational chirality, so as to result in the formation of hierarchical helical superstructures through twisting and bending of crystallites as shown in b). Also, to achieve the minimum energetic state, the helical superstructures may scroll to form the tubular morphology as illustrated in c).

## 3. Conclusions

The formation of hierarchical superstructures with helical sense in the self-assembly of achiral banana-shaped liquid crystalline molecules, BC7, in the THF/$H_2O$ solution corresponded well with the induction of optical activity, as evidenced by time-resolved CD experiment. There was no intrinsic chirality for a single-chain molecule of achiral BC7 whereas the self-assembled hierarchical superstructures in the solution exhibited specific optical activity after the occurrence of aggregation. The formed hierarchical superstructures were observed by TEM, SEM, and SPM at which hierarchical morphologies with helical sense can be clearly identified. Furthermore, the helical superstructure is attributed to the twisting and bending mechanism, as evidenced by SAED experiments, so as to lead the curving of the lamellar crystal. These interesting observations indicate that the self-assembly of specific molecular geometry gives rise to the formation of helical superstructures resulting from helical chain conformation.

## 4. Experimental

*Characterization*: The calorimetric measurements were carried out in Perkin-Elmer DSC 7 equipped with controlled cooling system in a flowing $N_2$ atmosphere. Temperature and heat flow scales at different scan rates (2.5, 5, 10, 20, 40 °C $min^{-1}$) were carefully calibrated with standard materials of cyclohexane and indium before experiments proceeded. Typically, the DSC sample weight was 5 mg to avoid a thermal gradient within the samples. The sample was first heated from 25 °C to 155 °C above their isotropic melting temperatures for 2 minutes to eliminate thermal history from the synthetic process. Then, the sample was cooled down to −5 °C, and then staying for 2 minutes, finally reheated again to 155 °C for the identification of corresponding thermal transitions. Optical textures of liquid crystal and crystalline phases at different temperatures were observed with an Olympus BX-60 equipped with a hot stage controlled by an INSTEC 200 central processor. It was carefully alignment before used, then were utilized to observe the thermal transitions and to analyze the optical textures. The micrographs were held isothermally at the temperature according to the transitions identified by DSC measurements. Also, the morphologies of self-assembled aggregates were observed under transmitted and depolarized mode. UV-Vis absorption spectra were recorded on a Hitachi U-3300 spectrophotometer. CD measurements were obtained from a JASCO J-715 spectrophotometer. UV and CD spectroscopic measurements were executed in order to study the specific interactions and the chiral expression in solution. For dilute THF solution, UV-Vis spectra were recorded in $10 \times 10$ mm quartz cuvettes whereas CD spectra were measured in quartz cuvettes with 1 mm light path. For time-resolved CD experiments, the o high tension (HT) voltage measurement was carried out simultaneously. The HT measurement is related to the total absorbance (A) of the sample, and the absorption spectra can be obtained from HT signals through the in-built Jasco software. In that case, the cylindrical quartz cuvette with 10 mm light path was used to load suitable volume of THF/$H_2O$ solution. TEM experiments were carried out in JEOL JEM-1200CXII at an accelerating voltage of 120 kV. Bright field TEM images were obtained using the mass-thickness contrast from shadowing. The samples were dropped on carbon film and supported by a 400 mesh Cu

ADVANCED FUNCTIONAL MATERIALS



grid, and then shadowed by Pt/Pb = 4/1 at 30° tilted to the surface. The electron diffraction (ED) experiments for the thin films were also carried out. Calibration of the ED spacing was done using TlCl in a *d* spacing smaller than 0.384 nm, which is the largest spacing for TlCl. Spacing values larger than 0.384 nm were calibrated by doubling the *d* spacing of those diffractions based on their first-order diffractions. SPM results by tapping mode were obtained from thin-film samples. A Seiko SPA-400 AFM with a SEIKO SPI-3800N probe station was employed at room temperature in ambient circumstance. A rectangle-shaped silicon tip was applied in dynamic force mode (DFM) experiments using a type of SI-DF20 with a spring force contact of 14 $Nm^{-1}$ and scan rate of 1 Hz. SEM images were performed on a JEOL JSM-5600 with accelerating voltages of 10 kV. The specimen was mounted to brass shims using carbon adhesive, and then sample surface was sputtered with gold (Au) in the vacuum evaporator. The molecular simulation was used by HyperChem 7 with the OPLS force field to examine the possible stable chain conformations.

*Sample Preparation*: Bulk sample was weighted with one milligram, and THF was used as solvent to dissolve it. Then, water was added in order to prepare the solution with mixed solvent of THF/$H_2O$. The mixed solution was then heated to higher temperature until the solution became transparent to eliminate fast crystallization (ca. 70 °C for five minutes). After complete dissolution, the solution was placed in the air at room temperature for the induction of aggregation (i.e., self-assembly). To trace the self-assembly process, the solution at the room temperature was examined at different times for aggregation. For spectroscopic experiments, time-resolved measurement was carried out on the prepared solution. Also, for morphological observation, the solution was dropped onto the glass slide or carbon-coated glass slide for casting at room temperature. After the evaporation of THF, the cast samples on carbon-coated glass slides were then examined for TEM whereas DPLM, SPM and SEM experiments were conducted on cast samples with glass slide substrates.

Received: May 7, 2008
Published online: October 22, 2008

[1] G. M. Whitesides, J. P. Mathias, C. T. Seto, *Science* **1991**, *254*, 1312.
[2] M. Muthukumar, C. K. Ober, E. L. Thomas, *Science* **1997**, *277*, 1225.
[3] J.-M. Lehn, *Science* **2002**, *295*, 2400.
[4] G. M. Whitesides, B. Grzybowski, *Science* **2002**, *295*, 2418.
[5] J. C. Nelson, J. G. Saven, J. S. Moore, P. G. Wolynes, *Science* **1997**, *277*, 1793.
[6] E. Yashima, K. Maeda, Y. Okamoto, *Nature* **1999**, *399*, 449.
[7] D. J. Hill, M. J. Mio, R. B. Prince, T. S. Hughes, J. S. Moore, *Chem. Rev.* **2001**, *101*, 3893.
[8] A. Petitjean, H. Nierengarten, A. V. Dorsselaer, J.-M. Lehn, *Angew. Chem. Int. Ed.* **2004**, *43*, 3695.
[9] J.-H. Fuhrhop, W. Helfrich, *Chem. Rev.* **1993**, *93*, 1565.
[10] J. J. L. M. Cornelissen, M. Fischer, N. A. J. M. Sommerdijk, R. J. M. Nolte, *Science* **1998**, *280*, 1427.
[11] J. H. Jung, H. Kobayashi, M. Masuda, T. Shimizu, S. Shinkai, *J. Am. Chem. Soc.* **2001**, *123*, 8785.
[12] W. Jin, T. Fukushima, M. Niki, A. Kosaka, N. Ishii, T. Aida, R. Noyori, *Proc. Natl. Acad. Sci. USA* **2005**, *102*, 10801.
[13] C. Y. Li, S. Z. D. Cheng, J. J. Ge, F. Bai, J. Z. Zhang, I. K. Mann, L.-C. Chien, F. W. Harris, B. Lotz, *J. Am. Chem. Soc.* **2000**, *122*, 72.
[14] C. Y. Li, S. Jin, X. Weng, J. J. Ge, D. Zhang, F. Bai, F. W. Harris, S. Z. D. Cheng, *Macromolecules* **2002**, *35*, 5475.
[15] R.-M. Ho, Y.-W. Chiang, C.-C. Tsai, C.-C. Lin, B.-T. Ko, B.-H. Huang, *J. Am. Chem. Soc.* **2004**, *126*, 2704.
[16] Y.-W. Chiang, R.-M. Ho, B.-T. Ko, C.-C. Lin, *Angew. Chem. Int. Ed.* **2005**, *44*, 7969.
[17] R.-M. Ho, C.-K. Chen, Y.-W. Chiang, B.-T. Ko, C.-C. Lin, *Adv. Mater.* **2006**, *18*, 2355.
[18] J. W. Goodby, M. A. Waugh, S. M. Stein, E. Chin, R. Pindak, J. S. Patel, *J. Am. Chem. Soc.* **1989**, *111*, 8119.
[19] J. W. Goodby, *Handbook of Liquid Crystals*, (Eds: D. Demus, J. W. Goodby, G. W. Gray, H.-W. Spiess, V. Vill), Wiley-VCH, Weinheim **1998**.
[20] H.-S. Kitzerow, C. Bahr, *Chirality in Liquid Crystals*, (Eds: L. Lam, E. M. Guyon, D. Langevin, H. E. Stanley), Springer, New York **2001**.
[21] K.-U. Jeong, S. Jin, J. J. Ge, B. S. Knapp, M. J. Graham, J. Ruan, M. Guo, H. Xiong, F. W. Harris, S. Z. D. Cheng, *Chem. Mater.* **2005**, *17*, 2852.
[22] K.-U. Jeong, B. S. Knapp, J. J. Ge, S. Jin, M. J. Graham, F. W. Harris, S. Z. D. Cheng, *Chem. Mater.* **2006**, *18*, 680.
[23] C.-H. Sung, L.-R. Kung, C.-S. Hsu, T.-F. Lin, R.-M. Ho, *Chem. Mater.* **2006**, *18*, 352.
[24] T.-F. Lin, R.-M. Ho, C.-H. Sung, C.-S. Hsu, *Chem. Mater.* **2006**, *18*, 5510.
[25] G. Pelzl, S. Diele, W. Weissflog, *Adv. Mater.* **1999**, *11*, 707.
[26] H. Takezoe, Y. Takanishi, *Jpn. J. Appl. Phys. Part 1*, **2006**, *45*, 597.
[27] R. A. Reddy, C. Tschierske, *J. Mater. Chem.* **2006**, *16*, 907.
[28] D. M. Walba, *Materials-Chirality 24*, (Eds: M. M. Green, R. J. M. Nolte, E. W. Meijer), John Wiley & Sons, Hoboken, NJ **2003**.
[29] G. Pelzl, I. Wirth, W. Weissflog, *Liq. Cryst.* **2001**, *28*, 969.
[30] S. Diele, G. Pelzl, W. Weissflog, *Liq. Cryst. Today* **1999**, *9*, 8.
[31] The nomenclature of the mesophases of the banana-shaped molecules such as $B_1$-$B_7$ was recommended at the International Workshop on Banana-Shaped Liquid Crystals: Chirality by Achiral Molecules organized by the Technical University in Berlin in December 1997.
[32] T. Niori, T. Sekine, J. Watanabe, T. Furukawa, H. Takezoe, *J. Mater. Chem.* **1996**, *6*, 1231.
[33] T. Sekine, Y. Takanishi, T. Niori, J. Watanabe, H. Takezoe, *Jpn. J. Appl. Phys. Part 2*, **1997**, *36*, L1201.
[34] D. R. Link, G. Natale, R. Shao, J. E. Maclennan, N. A. Clark, E. Körblova, D. M. Walba, *Science* **1997**, *278*, 1924.
[35] W. Weissflog, Ch, Lischka, I. Benné, T. Scharf, G. Pelzl, S. Diele, H. Kruth, *Proc. SPIE-Int. Soc. Opt. Eng.* **1998**, *3319*, 14.
[36] M. Zennyoji, Y. Takanishi, K. Ishikawa, J. Thisyukta, J. Watanabe, H. Takezoe, *J. Mater. Chem.* **1999**, *9*, 2775.
[37] D. M. Walba, E. Körblova, R. Shao, J. E. Maclennan, D. R. Link, M. A. Glaser, N. A. Clark, *Science* **2000**, *288*, 2181.
[38] D. Shen, A. Pegenau, S. Diele, I. Wirth, C. Tschierske, *J. Am. Chem. Soc.* **2000**, *122*, 1593.
[39] M. Zennyoji, Y. Takanishi, K. Ishikawa, J. Thisyukta, J. Watanabe, H. Takezoe, *Jpn. J. Appl. Phys. Part 1* **2000**, *39*, 3536.
[40] R. A. Reddy, M. W. Schröder, M. Bodyagin, H. Kresse, S. Diele, G. Pelzl, W. Weissflog, *Angew. Chem. Int. Ed.* **2005**, *44*, 774.
[41] T. Sekine, T. Niori, J. Watanabe, T. Furukawa, S. W. Choi, H. Takezoe, *J. Mater. Chem.* **1997**, *7*, 1307.
[42] J. Thisayukta, Y. Nakayama, S. Kawauchi, H. Takezoe, J. Watanabe, *J. Am. Chem. Soc.* **2000**, *122*, 7441.
[43] J. Thisyukta, H. Takezoe, J. Watanabe, *Jpn. J. Appl. Phys. Part 1*, **2001**, *40*, 3277.
[44] F. Araoka, N. Y. Ha, Y. Kinoshita, B. Park, J. W. Wu, H. Takezoe, *Phys. Rev. Lett.* **2005**, *94*, 137801.
[45] G. Pelzl, S. Diele, A. Jákli, Ch, Lischka, I. Wirth, W. Weissflog, *Liq. Cryst.* **1999**, *26*, 135.
[46] A. Jákli, C. Lischka, W. Weissflog, G. Pelzl, A. Saupe, *Liq. Cryst.* **2000**, *27*, 1405.

  

[47] H. N. S. Murthy, B. K. Sadashiva, *Liq. Cryst.* **2003**, *30*, 1051.
[48] D. A. Coleman, J. Fernsler, N. Chattham, M. Nakata, Y. Takanishi, E. Körblova, D. R. Link, R.-F. Shao, W. G. Jang, J. E. Maclennan, O. Mondainn-Monval, C. Boyer, W. Weissflog, G. Pelzl, L.-C. Chien, J. Zasadzinski, J. Watanabe, D. M. Walba, H. Takezoe, N. A. Clark, *Science* **2003**, *301*, 1204.
[49] G. Pelzl, M. W. Schröder, U. Dunemann, S. Diele, W. Weissflog, C. Jones, D. Coleman, N. A. Clark, R. Stannarius, J. Li, B. Das, S. Grande, *J. Mater. Chem.* **2004**, *14*, 2492.
[50] T. Sekine, T. Niori, M. Sone, J. Watanabe, S.-W. Choi, Y. Takanishi, H. Takezoe, *Jpn. J. Appl. Phys. Part 1* **1997**, *36*, 6455.
[51] E. Gorecka, M. Nakata, J. Mieczkowski, Y. Takanishi, K. Ishikawa, J. Watanabe, H. Takezoe, S. H. Eichhorn, T. M. Swager, *Phys. Rev. Lett.* **2000**, *85*, 2526.
[52] T. Imase, S. Kawauchi, J. Watanabe, *J. Mol. Struct.* **2001**, *560*, 275.
[53] J. Thisyukta, H. Niwano, H. Takezoe, J. Watanabe, *J. Am. Chem. Soc.* **2002**, *124*, 3354.
[54] H. Kurosu, M. Kawasaki, M. Hirose, M. Yamada, S. Kang, J. Thisayukta, M. Sone, H. Takezoe, J. Watanabe, *J. Phys. Chem. A* **2004**, *108*, 4674.
[55] H. Niwano, M. Nakata, J. Thisyukta, D. R. Link, H. Takezoe, J. Watanabe, *J. Phys. Chem. B* **2004**, *108*, 14889.
[56] J. Watanabe, T. Niori, T. Sekine, H. Takezoe, *Jpn. J. Appl. Phys. Part 2* **1998**, *37*, L139–L142.
[57] G. Heppke, D. Moro, *Science* **1998**, *279*, 1872.
[58] D. M. Walba, E. Korblova, C.-C. Huang, R. Shao, M. Nakata, N. A. Clark, *J. Am. Chem. Soc.* **2006**, *128*, 5318.
[59] D. M. Walba, L. Eshdat, E. Körblova, R. K. Shoemaker, *Cryst. Growth Des.* **2005**, *5*, 2091.
[60] K. Sayama, S. Tsukagoshi, K. Hara, Y. Ohga, A. Shinpou, Y. Abe, S. Suga, H. Arakawa, *J. Phys. Chem. B* **2002**, *106*, 1363.
[61] H. Isago, *Chem. Commun.* **2003**, 1864.
[62] K. Adachi, K. Chayama, H. Watarai, *Langmuir* **2006**, *22*, 1630.
[63] T. Miyagawa, M. Yamamoto, R. Muraki, H. Onouchi, E. Yashima, *J. Am. Chem. Soc.* **2007**, *129*, 3676.
[64] M. S. Spector, J. V. Selinger, A. Singh, J. M. Rodriguez, R. R. Price, J. M. Schnur, *Langmuir* **1998**, *14*, 3493.
[65] J. V. Selinger, M. S. Spector, J. M. Schnur, *J. Phys. Chem. B* **2001**, *105*, 7157.
[66] M. M. Green, B. A. Garetz, B. Munoz, H.-P. Chang, *J. Am. Chem. Soc.* **1995**, *117*, 4181.
[67] M. M. Green, J.-W. Park, T. Sato, A. Teramoto, S. Lifson, R. L. B. Selinger, J. V. Selinger, *Angew. Chem. Int. Ed.* **1999**, *38*, 3138.
[68] J. V. Gestel, *Macromolecules* **2004**, *37*, 3894.
[69] N. Nakashima, S. Asakuma, T. Kunitake, *J. Am. Chem. Soc.* **1985**, *107*, 509.
[70] F.-H. Fuhrhop, P. Schnieder, E. Boekema, W. Helfrich, *J. Am. Chem. Soc.* **1988**, *110*, 2861.
[71] O.-Y. Zhong-can, L. Ji-xing, *Phys. Rev. Lett.* **1990**, *65*, 1679.
[72] O.-Y. Zhong-can, L. Ji-xing, *Phys. Rev. A* **1991**, *43*, 6826.
[73] J. V. Selinger, J. M. Schnur, *Phys. Rev. Lett.* **1993**, *71*, 4091.